Real-Gas Effect on Fluid Injection: A Numerical and Experimental Study

By N. Vallée, U. Guven, J.-B. Blaisot AND G. Ribert

CORIA - CNRS, Normandie Univ., INSA Rouen Normandie, UNIROUEN
76000 Rouen, France

When the chamber pressure exceeds the critical pressure of working fluids, the supercritical state of matter is reached and the distinction between gas and liquid becomes blurred. For such special conditions, experimental data are scarce and need to be consolidated. In the present study, the results obtained from the experiment REFINE (Real-gas Effect on Fluid Injection: a Numerical and Experimental study) are analyzed and a first attempt to reproduce them by numerical simulation is performed. In REFINE, an injection of Ethane into Nitrogen under sub- and supercritical conditions is performed. The ambient gas pressure can be raised up to 6.0 MPa and warmed up to 323 K to scan sub- and trans-critical injections. The chamber is equipped with two perpendicular optical access for simultaneous diagnostics. Experimental data are collected from shadowgraph and diffused backlight illumination techniques. Quantitative measurements of jet spreading angle and breakup length are compared to results coming from literature.

1. Introduction

Mixing is one of the most important phenomena in combustion devices because it determines combustion efficiency and stability along with heat transfer characteristics. In addition, most of the current understanding of turbulence and mixing is the result of atmospheric-pressure studies and numerous numerical and experimental databases are available. A similar work has then to be undertaken for sub-, trans- and super-critical flows investigation, i.e. real-gas effects have to be considered. Indeed, this research field lacks of experimental data, useful for the numerical code validation. Even if simulation has made serious progress in the last decade, numerical codes still need well-documented experimental test cases for validation. Indeed, at supercritical state, the fluid is neither a liquid nor a gas, but may have liquid-like density with gas-like properties: beyond the critical point (Pc,Tc), there is no distinction between gaseous and liquid phases for pure species. In the case of mixing, depending on the considered species, defining the state of matter becomes much more complicated [1] and modeling turbulence, mixing and combustion is still a challenge [2].
The topic addressed in this project is focused on the current research program REFINE that is held at CORIA Lab and that considers the experimental investigation and numerical simulation of real-fluid injection and mixing processes under sub-, trans- and supercritical conditions. The domain of interest of REFINE is the propulsion with application to the automotive and aerospace science and technology where supercritical fluids may be considered as propellants. Indeed, the need for higher efficiency and lower emission levels leads to increase pressure and temperature levels, i.e. to reach supercritical

properties of fluids. The objective of REFINE is to build a simple well-controlled test-bench able to study a fluid injection under sub-, trans- and super-critical conditions and to associate experimental and numerical diagnostics to deliver the finest information. An ethane injection is then considered in a 5-liter high-pressure experimental chamber.
The reference experiment REFINE is detailed in section 2 and the results obtained with shadowgraph and diffuse backlight illumination techniques are given in section 3. A first attempt to simulate this configuration is given in section 4.

2. Reference experiment

The experiment has been designed to study injection and atomization of a non-assisted jet under high pressures conditions. REFINE test bench is equipped with a steel chamber able to withstand pressures up to 10 MPa and moderate temperatures (573 K). Two optical axes through circular silica windows of $d = 120$ mm are available for simultaneous measurements (see Fig. 1). The chosen working fluids are Ethane (C_2H_6, $T_c = 305.3$ K and $p_c = 4.87$ MPa) and Propane (C_3H_8, $T_c = 369.8$ K and $p_c = 4.25$ MPa). Their moderate critical pressure and temperature are within the range of operating conditions achievable in the chamber. A one-liter pump supplies the working fluid at the liquid-gas equilibrium pressure. Before injection, the pump is filled up, and then the fluid contained inside the vessel of the pump is compressed to the target pressure plus 0.05 MPa to prevent the ambient fluid in the main chamber from entering the pump and creating an effervescent jet.

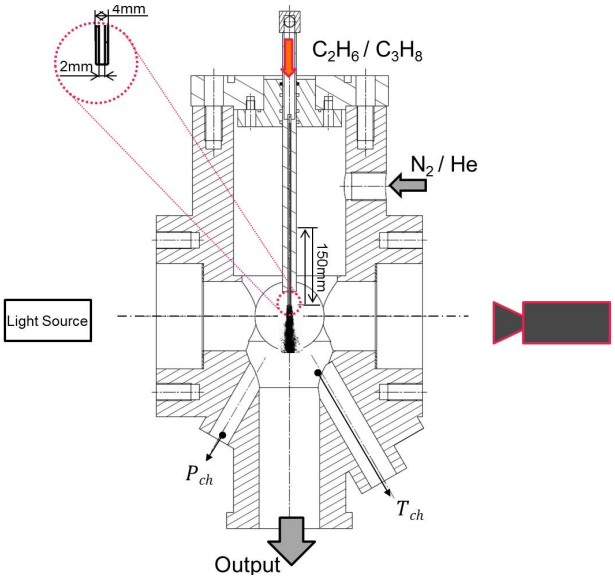

FIGURE 1. REFINE injection chamber.

The injection is performed with a sharp-edged stainless steel tube of 210 mm long, with a 4 mm outer diameter and a 2 mm inner diameter. The injector can be moved vertically over a 150 mm stroke by a motorized system located on the top of the chamber, to explore the jet further downstream. The rig is fully instrumented with thermocouples, pressure gauges and mass flow meters as indicated in Fig. 2. The chamber is filled with Nitrogen and the pressure is controlled with a pressure regulator having a precision

of ± 0.1 MPa. To warm up the ambient fluid, two Mica heating plates are placed at the bottom of the chamber and a heater (Fig. 2) is inserted just before the feeding of N_2.

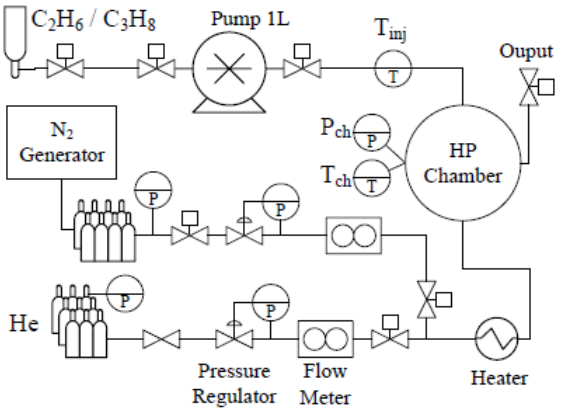

FIGURE 2. Flowchart of REFINE test bench.

Two optical diagnostics, diffused back-light illumination (DBI) and shadowgraphy, are used to quantify the injection and atomization of the working fluids. The main difference between these two techniques lies in the light source arrangement. For shadowgraph, a collimated laser diode (Cavitar) is used whereas a stroboscope flash-lamp (MVS-2601) with a glass diffuser is used for DBI. The DBI allows for detecting the largest density gradients, which are essentially located at the liquid-gas interface contrary to shadowgraph that detects smoother density gradient.

3. Post-processing experimental images

A set of images using the shadowgraph and DBI techniques has been recorded for various inlet velocities, temperature (T_{ch}) and pressure (P) in the chamber. In the present cases, P varies from 4.0 to 6.0 MPa and $T_{ch} = 293$ K or $T_{ch} = 323$ K. The results for injection of ethane into nitrogen are shown in Fig. 3 and 4, for a chamber pressure P = 6.0 MPa.

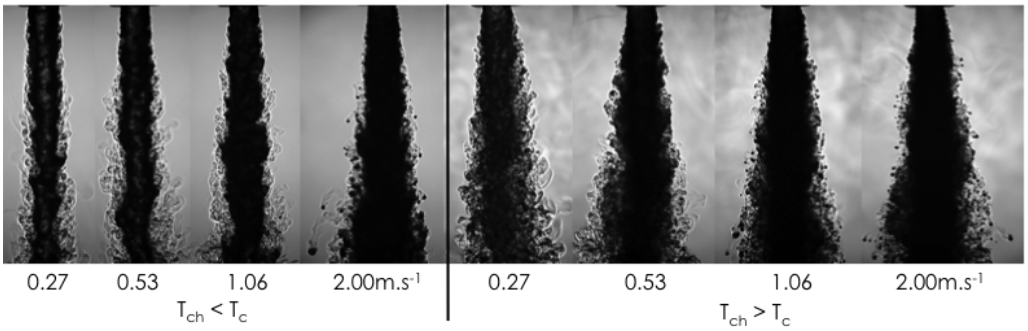

FIGURE 3. Shadowgraphs of ethane into nitrogen at $P = 6.0$ MPa.

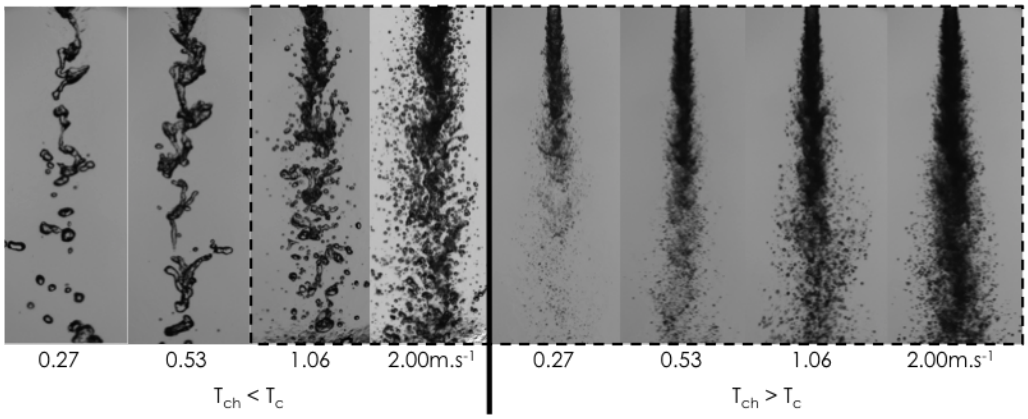

FIGURE 4. DBI of ethane into nitrogen at $P = 6.0$ MPa.

3.1. *Spreading Angle*

The spreading angle is evaluated from shadowgraphs, based on the localization of the C_2H_6/N_2 mixing layer. As it can be seen on the raw image in Fig. 5, the background illumination is not homogeneous, i.e. darker in the corners and lighter in the center. Raw images are normalized to correct these defects and obtain a uniform background. Then, images are binarized with a threshold level chosen to separate the jet of ethane from the ambient nitrogen. The mixing layer region is determined by calculating the

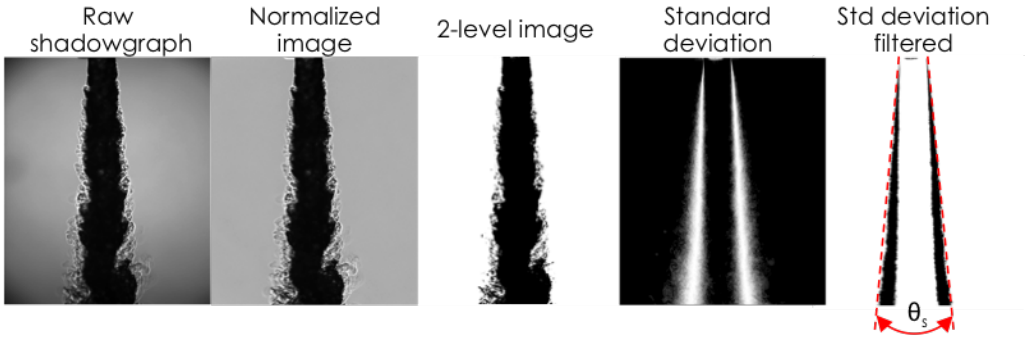

FIGURE 5. Steps of post processing for the spreading angle, θ_S.

standard deviation from 120 binarized images. A second threshold is then applied to get clear boundaries of the mixing layer region. Applying a linear regression on these regions yields the slope indicated by the two lines in Fig. 5, giving the spreading angle, (θ_S). This technique is repeated for all operating conditions and the spreading angles are plotted in Fig. 6 against the density ratio ρ_{ch}/ρ_{jet}, with ρ_{ch}, the density of N_2 and ρ_{jet}, the density of C_2H_6. Increasing the velocity injection of C_2H_6 or the pressure in the chamber leads to an increase of $\theta_S, \forall T_{ch}$. These results are in agreement with the observations of Mayer et al. [4]. Results from Cherhroudi et al. [3] for an injection of liquid N_2 into gaseous N_2 are also plotted in Fig. 6, showing a similar trend.

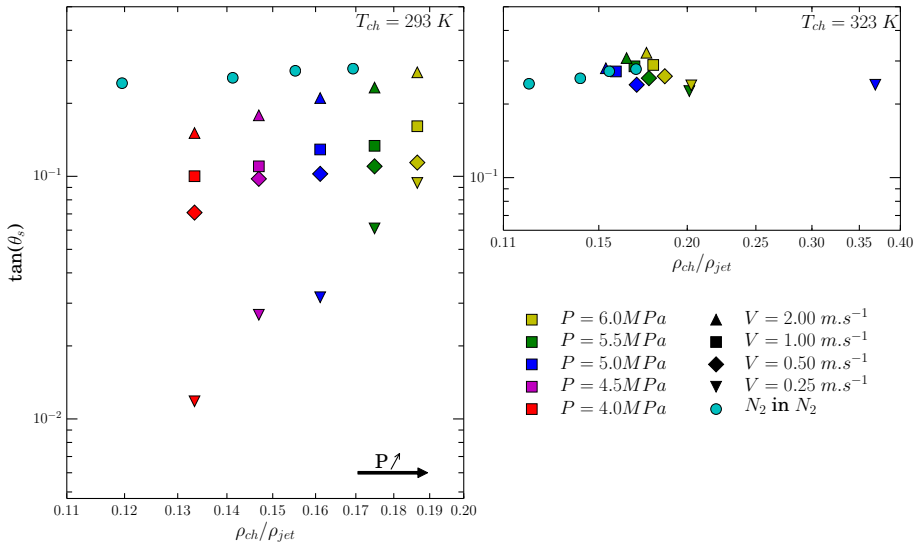

FIGURE 6. Spreading angle versus the chamber to injectant density ratio. For comparison, spreading angle (θ_S) for injection of liquid N_2 into N_2 at ambient temperature from Fig. 8 of Chehroudi?s paper [3] are added for comparison.

3.2. *Dark core length*

The dark core length is estimated from DBI technique that highlights the strongest gradients in the flow. In the particular case of a liquid injection, an interface can be clearly determined contrary to supercritical cases where a diffuse mixing layer between the dense and light fluids may occur. As shown in Fig. 4, two types of jet structure are observed. For the two lowest velocities at ambient temperature ($T_{ch} < T_c$), the first discontinuity in the jet can be clearly identified and measured directly on raw images. This measurement will be called breakup length L_{Bu}. For other conditions, i.e. inside the dashed rectangle in Fig. 4, a cloud of drops does not make possible this direct measurement and a probability approach is used to deliver the dark core length, L_{Dc}.

Evaluating the breakup length follows the methodology used to evaluate the spreading angle. A threshold is accurately chosen to delineate the interface of the continuous object attached to the injectors lips. This point is highlighted in Fig. 7 for a jet identified in second wind-induced regime [5]. Such a procedure is performed for 600 raw images to obtain probability density function (pdf) of L_{Bu}. In Fig. 8), the shortest breakup length is found for $V = 0.25$ m/s and L_{Bu} increases with the discharge velocity. The pdf of L_{Bu} are wider for the largest velocity and for $V = 0.25$ m/s the maximum peak is better defined. Finally, increasing the pressure in the chamber slightly reduced L_{Bu}.

Considering an atomized jet, i.e. when the liquid injection leads to a cloud of drops, the different steps of post-processing are still the same except that an average of 600 continuous object images is computed (see Fig. 9) for the same injection conditions. Finally, a second threshold is used to define the most probable dark core length (L_{Dc}). The dark core length L_{Dc} is plotted against the inlet velocity in Fig. 10. The breakup length determined for the two lower velocities at ambient temperature are also indicated on the graph, showing the same range of values and thus making the analysis consistent. The dark core length growths with the inlet velocity regardless the pressure in the chamber and the ambient temperature under consideration. When L_{Dc} reaches

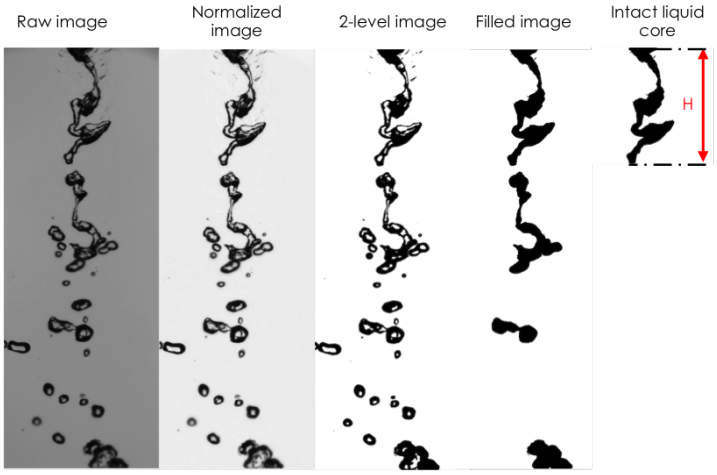

FIGURE 7. Methodology for post processing the breakup length, $H \equiv L_{Bu}$.

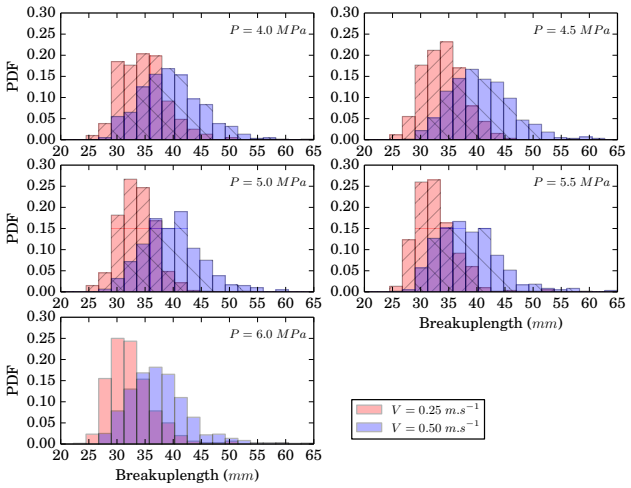

FIGURE 8. Probability density function (pdf) of L_{Bu} given in mm with $T_{ch} = 293$ K.

zero, a gaz jet were observed during the injection. As for the calculation of L_{Bu} when $V = 0.25$ m/s, increasing the pressure in the chamber slightly decreases the dark core length at $T_{ch} = 293$ K. A clear conclusion cannot be drawn for the other inlet velocities. Switching the temperature of nitrogen from $T_{ch} = 293$ K to $T_{ch} = 323$ K shiftes the values of L_{Bu} about 10 mm. Also, the cases $P = 5.0$ MPa with $V = 0.25$ m/s or $V = 0.50$ m/s have values of L_{Bu} lower than expected compared to the cases with $T_{ch} = 293$ K.

4. Numerical simulations

The simulations presented thereafter have been performed using the parallel solver SiTCom-B (`https://www.coria-cfd.fr/index.php/SiTCom-B`) that solves the fully compressible Navier-Stokes equations for multi-species reacting flows. SiTCom-B is based

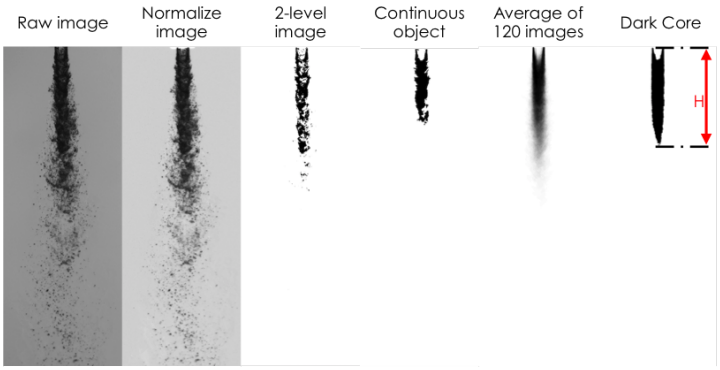

FIGURE 9. Methodology of post processing the dark core length, $H \equiv L_{Dc}$.

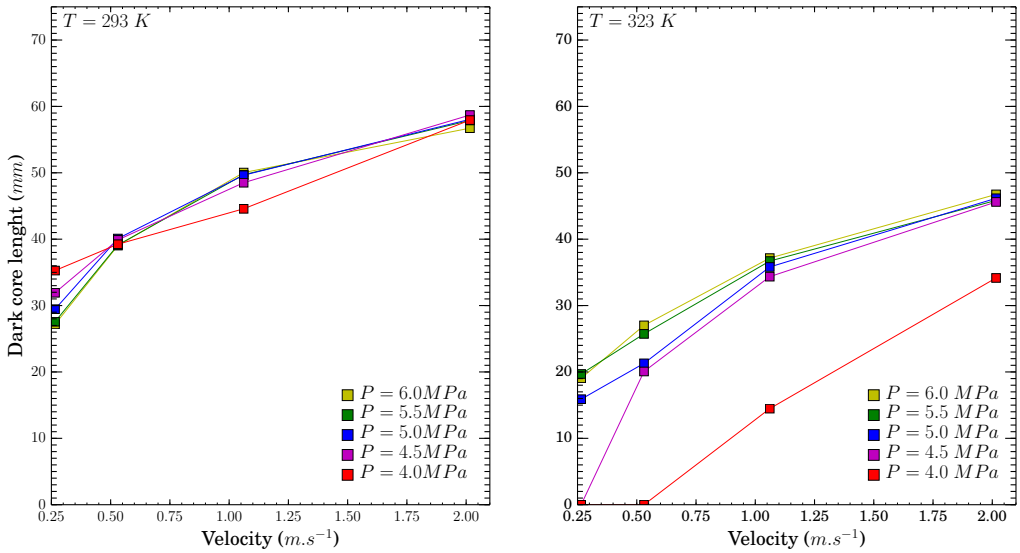

FIGURE 10. Dark core length plotted against the inlet velocity.

on an explicit finite volumes scheme written for cartesian grids. The convective terms are computed resorting to a fourth-order centered skew-symmetric-like scheme [6] and the diffusive terms are computed using a fourth-order centered scheme. Time integration is performed using a fourth order Runge-Kutta method [7, 8]. The spatial discretization scheme is augmented by a blend of second- and fourth-order artificial dissipation terms [9–11]; these terms are added in order to suppress spurious oscillations and damp high-frequency modes. A sensor based on pressure and density gradients insures that the artificial dissipation is applied only to zones of interest, *i.e.* where either strong gradients of density or pressure, which cannot be resolved by the mesh, are detected [12]. The Navier-Stokes characteristic boundary condition formalism developed by Petit et al. [12] in the context of fluids featuring real-gas effects is used.

To simulate supercritical flows, SiTComb-B numerical code features real gas thermodynamic [13, 14]. A cubic equation of state (EoS) replaces the classical ideal gas law,

linking the pressure, p, temperature, T and density, ρ, as

$$p = \frac{\rho R_u T}{W - b\rho} - \frac{\rho^2 a\alpha(T,\omega)}{W^2 + ubW\rho + wb^2\rho^2}, \tag{4.1}$$

where R_u is the universal gas constant and W the molecular weight of the fluid mixture, $W = \sum_{k=1}^{N_{\text{sp}}} X_k W_k$ with X_k the mole fraction of species k (among N_{sp} species). u and w in Eq. (4.1) are chosen according to the desired model of EoS, i.e. the Peng-Robinson (PR) EoS in this study ($u = 2$ and $w = -1$ [15]). The Van der Waals mixing rules are used for mixtures: $a\alpha = \sum_{i=1}^{N_{\text{sp}}} \sum_{j=1}^{N_{\text{sp}}} X_i X_j \sqrt{\alpha_i \alpha_j a_i a_j}(1 - \kappa_{ij})$ and $b = \sum_{i=1}^{N_{\text{sp}}} X_i b_i$. κ_{ij} is the binary interaction coefficient. The constants a_i (attractive forces), b_i (co-volume of particles) and α_i are determined from universal relationships [15], involving the critical temperature and partial pressure of species k, T_{c_k} and p_{c_k}, respectively, as well as the acentric factor, which quantifies the deviation from the spherical symmetry in a molecule.

SiTComb-B numerical code [12, 16, 17] solves the fully coupled conservation equations of momentum, species and energy. In what follows, u_i is the velocity component in the x_i-axis (spatial coordinate), t is the time and ρ the density.

• Assuming a newtonian fluid and neglecting the volume forces, the equation of momentum is written:

$$\frac{\partial(\rho u_i)}{\partial t} + \frac{\partial}{\partial x_j}(\rho u_j u_i) = \frac{\partial \sigma_{ij}}{\partial x_j}, \tag{4.2}$$

with the stress tensor, σ_{ij}, expressed with the viscous tensor, τ_{ij}, and pressure, p: $\sigma_{ij} = \tau_{ij} - p\delta_{ij}$. δ_{ij} is the Kronecker symbol. In Eq. (4.2), the viscous tensor is given by

$$\tau_{ij} = \left(\kappa - \frac{2}{3}\mu\right)\frac{\partial u_k}{\partial x_k}\delta_{ij} + \mu\left(\frac{\partial u_i}{\partial x_j} + \frac{\partial u_j}{\partial x_i}\right), \tag{4.3}$$

where μ denotes the molecular dynamic viscosity and κ the bulk viscosity, which depends on the local properties of the fluid. In this study, the bulk viscosity is neglected and $\kappa = 0$.

• The mass conservation equation for species k in a pool of N_{sp} species is written:

$$\frac{\partial(\rho Y_k)}{\partial t} + \frac{\partial}{\partial x_j}(\rho(u_j + V_{k,j})Y_k) = 0, \tag{4.4}$$

where Y_k is the mass fraction of species k and $\rho = \sum_{k=1}^{N_s} \rho Y_k$. $V_{k,j}$ is the j^{th} component of the diffusion velocity $\mathbf{V_k}$ of species k.

• The energy equation is written for the total non chemical energy (E), i.e. the sum of sensible energy and kinetic energy, as

$$\frac{\partial(\rho E)}{\partial t} + \frac{\partial}{\partial x_j}(\rho u_j E) = \frac{\partial q_j}{\partial x_j} + \frac{\partial}{\partial x_j}(\sigma_{ij} u_i), \tag{4.5}$$

The heat flux vector required in Eq. (4.5) for a multi-component flow is given by

$$\mathbf{q} = \lambda \nabla T + \rho \sum_{k=1}^{N_{\text{sp}}} h_{s,k} Y_k \mathbf{V}_k. \tag{4.6}$$

λ is the thermal conductivity of the mixture and $h_{s,k}$, the sensible enthalpy of species k. Classical techniques used to evaluate transport properties (viscosity, μ, and thermal conductivity, λ) are replaced by accurate high-pressure relations proposed by Chung *et*

al. [18], which extends the Chapman-Enskog theory by introducing a dense-fluid correction. Neglecting the baro-diffusion effects, the expression for diffusion velocity of species k in the mixture, which appears in Eq. (4.4) and (4.6), is written as,

$$\mathbf{V}_k = -\sum_{l=1}^{N_{\text{sp}}} D_{kl} \nabla X_l, \tag{4.7}$$

with D_{kl}, the multi-component diffusion coefficients, and X_l, the mole fraction of species l. A high-pressure correction is applied to the evaluation of D_{kl} [19].

The case under study from the REFINE experiment corresponds to a supercritical injection of ethane into nitrogen at $V = 1.0$ m/s, $T_{ch} = 323$ K and $P = 6.0$ MPa.The modeling of the two-dimensional target configuration is shown in Fig. 11 where ethane is injected from the left to the right. A 1/7th power law for the inlet velocity of ethane is used to mimic the mean velocity profile in a turbulent pipe flow. The computational domain is

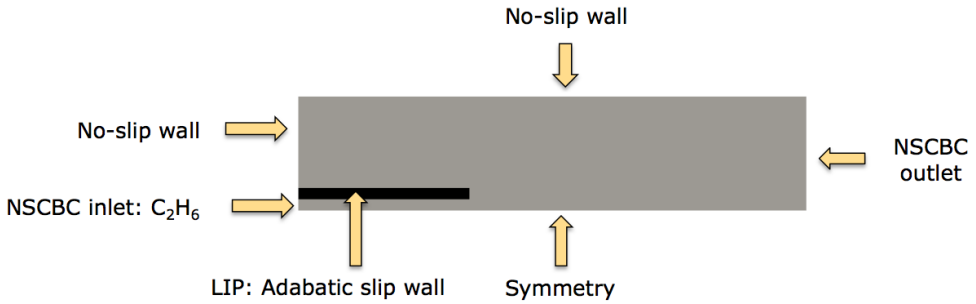

FIGURE 11. Target configuration with boundary conditions.

$45h$ long in the axial direction and extends over $10h$ in the transverse direction, with h, the injector lip. A constant mesh size of $\Delta_x = 50$ μm is used. And finally simulations are carried out with a mesh which contains 180.000 cells. The instantaneous fields of pressure, velocities and ethane mass fraction are provided in Fig. 12. The background pressure of 6.0 MPa is well recovered by simulations and a mixing layer between the ambient nitrogen and ethane develops naturally. The impact of the boundary condition at the top of the domain of calculation (no-slip wall) has an unexpected impact on the flow development, promoting a backward velocity and artificially thickening the mixing layer. Consequently, the average field of ethane (Fig. 13) exhibits an experimental spreading angle ($\theta_S^{Exp} \approx 0.11$ rad) wider than in the simulation ($\theta_S^{Num} \approx 0.09$ rad). Statistics have been recorded for 10 convective times, i.e. $10T_{conv}$ with $T_{conv} = 90$ ms.

5. Conclusions

A new fully instrumented experimental test-bench has been developed at CORIA lab to study the injection of inert fluids under supercritical conditions. In this study, Ethane is injected into a cold or warm environment of Nitrogen. The knowledge of the behavior of those fluids has been detailed. Results for the breakup length and the spreading angle are in agreement with the literature. It has been shown that the temperature of the ambient fluid played a major role in jet disintegration when pressure exceeds the critical pressure of the injected fluid. In case of an ambient temperature higher than the critical

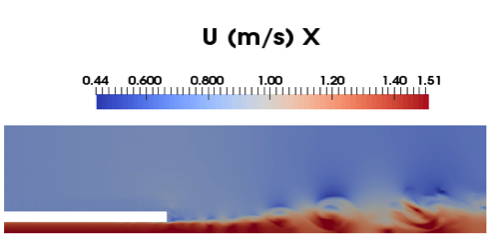

(a) Axial velocity field.

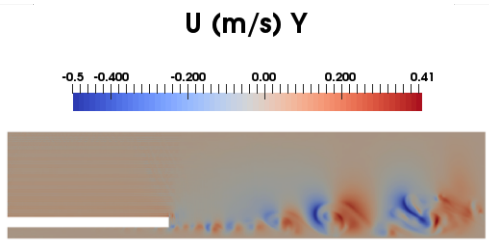

(b) Transverse velocity field.

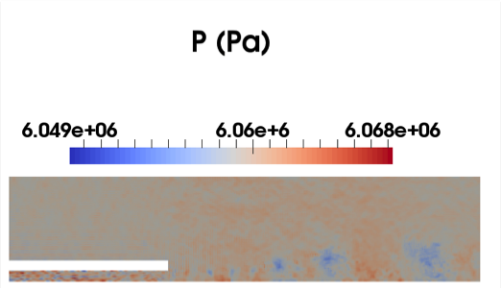

(c) Pressure field.

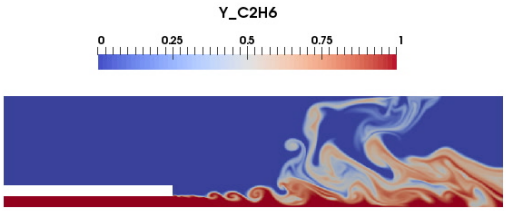

(d) C_2H_6 mass fraction.

FIGURE 12. Instantaneous fields at $t = 10T_{conv}$.

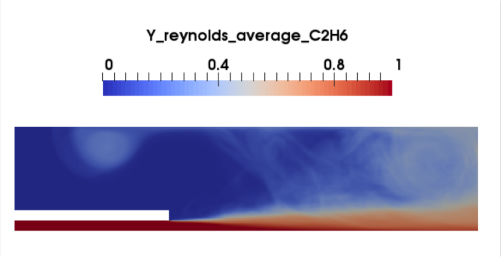

FIGURE 13. Reynolds average field of ethane.

temperature of injected fluids a diffuse mixing process occurs for low discharge velocities. For a higher injection velocities, a process of atomization appears but with a larger spatial distribution of drops. These results were obtained by shadowgraphy and diffused backlight illumination that gave complementary information. The numerical simulation performed for the supercritical case exhibited a shorter spreading angle compared to the value from experiment, certainly because of the modeling of the outlet on side. Also,

a fully three-dimensional geometry with a modeling comprising a multiphase approach should be performed to come closer to the real configuration.

Acknowledgments

Financial support has been provided by the German Research Foundation (Deutsche Forschungsgemeinschaft – DFG) in the framework of the Sonderforschungsbereich Transregio 40. Computational resources have been provided by the High Performance Computing Center Stuttgart (HLRS).

The research project REFINE (Real-gas Effects on Fluid Injection: a Numerical and Experimental study) is supported by the ANR (Agence Nationale de la Recherche) under the Grant No. ANR-13-BS09-0007.

References

[1] VAN KONYNENBURG, P. AND SCOTT, R. (1980). Critical lines and phase equilibria in binary van der waals mixtures. *Philosophical Transactions of the Royal Society of London A: Mathematical, Physical and Engineering Sciences*, **298**(1442), 495–540.

[2] BELLAN, J. (2000). Supercritical (and subcritical) fluid behaviour and modeling : drops, streams, shear, and mixing layers, jets, and sprays. *Prog. Energy Combust. Sci.*, **26**, 329–366.

[3] CHEHROUDI, B., TALLEY, D., MAYER, W., BRANAM, R. AND SMITH, J. (2003). *Understanding injection into high pressure supercritical environments*. Tech. rep., DTIC Document.

[4] MAYER, W. AND TELAAR, J. (2002). Investigation of breakup of turbulent cryogenic variable-density jets. *Atomization and Sprays*, **12**(5&6).

[5] DUMOUCHEL, C. (2008). On the experimental investigation on primary atomization of liquid streams. *Exp. Fluids*, **45**, 371–422.

[6] DUCROS, F., FERRAND, V., NICOUD, F., WEBER, C., DARRACQ, D., GACHERIEU, C. AND POINSOT, T. (1999). Large-eddy simulation of the shock/turbulence interaction. *J. Comput. Phys.*, **152**(2), 517–549.

[7] JIANG, G. AND SHU., C. (1996). Efficient implementation of weighted ENO schemes. *J. Comput. Phys.*, **126**, 73–85.

[8] GOTTLIEB, S. AND SHU, C. (1998). Total variation diminishing Runge-Kutta schemes. *Math. Comput.*, **67**(221), 73–85.

[9] TATSUMI, S., MARTINELLI, L. AND JAMESON, A. (1995). Flux-limited schemes for the compressible Navier-Stokes equations. *AIAA J.*, **33**(2), 252–261.

[10] SWANSON, R. AND TURKEL, E. (1992). On central-difference and upwind schemes. *J. Comput. Phys.*, **101**(2), 292–306.

[11] SWANSON, R., RADESPIEL, R. AND TURKEL, E. (1998). On some numerical dissipation schemes. *J. Comput. Phys.*, **147**(2), 518–544.

[12] PETIT, X., RIBERT, G., DOMINGO, P. AND LARTIGUE, G. (2013). Large-eddy simulation of supercritical fluid injection. *J. Supercritical Fluids*, **84**, 61–73.

[13] RIBERT, G., TAIEB, D., PETIT, X., LARTIGUE, G. AND DOMINGO, P. (2012). Simulation of supercritical flows in rocket-motor engines: application to cooling channel and injection system. *EUCASS Book Series*, **4**, 205–226.

[14] RIBERT, G., PETIT, X. AND DOMINGO, P. (2017). High-pressure methane-oxygen flames. Analysis of sub-grid scale contributions in filtered equations of state. *J. Supercritical Fluids*, **121**, 78–88.

[15] POLING, B., PRAUSNITZ, J. AND O'CONNELL, J. (2001). *The properties of gases and liquids*. 5th edn. McGraw Hill.

[16] BOUHERAOUA, L., DOMINGO, P. AND RIBERT, G. (2017). Large eddy simulation of a supersonic lifted jet flame: Analysis of the turbulent flame base. *Combust. Flame*, **179**, 199–318.

[17] GUVEN, U. AND RIBERT, G. (2017). Large-eddy simulation of supersonic H_2/O_2 combustion: application to a rocket-like igniter. *J. Propul. Power (in press)*.

[18] CHUNG, T., AJLAN, M., LEE, L. AND STARLING, K. (1988). Generalized multiparameter corresponding state correlation for polyatomic, polar fluid transport properties. *Industrial and Engineering Chemistry Research*, **27**, 671–679.

[19] TAKAHASHI, S. (1974). Preparation of a generalized chart for the diffusion coefficient of gases at high pressures. *J. Chem. Eng. Jap.*, **7**, 417–420.